IEEE Access
Multidisciplinary | Rapid Review | Open Access Journal

Received 7 December 2023, accepted 20 December 2023, date of publication 19 January 2024,
date of current version 25 January 2024.

Digital Object Identifier 10.1109/ACCESS.2024.3356358

APPLIED RESEARCH

Reconfigurable Antenna Array Testbed for Quantized Controlling

MICHAL POKORNY[1], IVO VERTAT[1], DAVID PANEK[2], (Member, IEEE), PAVEL HAZDRA[3], (Member, IEEE), MILAN SVANDA[3], JAN KRACEK[3], (Member, IEEE), MILOS MAZANEK[3], (Life Senior Member, IEEE), JIRI MASOPUST[4], AND PAVEL KARBAN[2], (Member, IEEE)

[1]Department of Electronics and Information Technology, University of West Bohemia, 306 14 Pilsen, Czech Republic
[2]Department of Electrical and Computational Engineering, University of West Bohemia, 306 14 Pilsen, Czech Republic
[3]Department of Electromagnetic Field, Czech Technical University in Prague, 166 27 Prague, Czech Republic
[4]Department of Computer Science and Engineering, University of West Bohemia, 306 14 Pilsen, Czech Republic

Corresponding author: Pavel Hazdra (hazdrap@fel.cvut.cz)

This work was supported by the Czech Science Foundation, Antenna Arrays with Quantized Controlling, under Grant 20-02046S.

ABSTRACT Contemporary beam-forming antenna arrays often use a large number of individual elements, sometimes hundreds or more, to achieve high gain for advanced applications like radar, space communication, and next-gen cellular networks. These arrays are complex and costly due to the need for precise amplitude and phase adjustments across the elements. The feeding network complexity leads to signal losses, reduced efficiency, and higher noise. Current research aims to simplify arrays, reduce active elements needing frontends, and streamline the feeding network, considering non-uniform, sparse, parasitic, or reflective arrays. Challenges arise from element coupling and imperfect models of high-frequency materials and electronic components. Therefore, in addition to simulations, practical experimentation remains vital. This paper focuses on designing a novel 3×3 element antenna array with digital quantized control. We explore the impact of quantized control on beamforming and plan to validate simplified orthogonal optimization methods with limited quantization depth. The proposed antenna array is applicable to 2400 MHz band research, including arrays with parasitic elements and switchable polarization for individual elements.

INDEX TERMS Antenna array, quantization, mutual coupling.

I. INTRODUCTION

Antenna arrays with beamforming are utilized in a wide range of applications. In the space industry, they serve as communications satellite antennas, creating multiple variable divergence beams to optimize service coverage on Earth [1], [2]. They are also used as highly directional antennas for deep space missions [3], [4]. Phased antenna arrays are relatively common in data terminals for aircrafts, ships, ground vehicles [5], [6] and even households requiring data connectivity via existing or planned satellite networks such as Starlink, OneWeb, Telesat, Hongyan, Hiber, Swarm, Astrocast, Kepler, Lacuna, Myriota, Fleetspace, etc. Several projects [7], [8] are also exploring the potential for their future use in traditional satellite ground stations. Unlike large parabolic antennas, these arrays would have the capability to simultaneously track and communicate with multiple satellites in different positions. In the area of the next-generation cellular networks, large antenna arrays can adaptively focus on a main beam or create and target multiple beams in areas with a concentration of customers demanding high-speed data services [9], [10]. Another significant application of phased antenna arrays is in ground and airborne radars, where they eliminate the need for mechanical steering and can simultaneously track multiple targets [11], [12].

Massive antenna arrays with limited dimensions feature a substantial number of mutually coupled elements and numerous ports equipped with attached RF frontends. These consist of phasing circuits, variable gain amplifiers, variable attenuators, power amplifiers, low noise amplifiers, RF switching relays, and more. The technological complexity, simulation intricacy, financial costs, and calibration challenges all

The associate editor coordinating the review of this manuscript and approving it for publication was Mohammed Bait-Suwailam.

escalate with the increasing number of actively controlled antenna array ports. Hence, a significant part of research is currently focused on simplifying antenna arrays by reducing the number of actively controlled elements. Additionally, research is addressing the challenges of calibration and auto-calibration for these antenna arrays.

In references [13] and [14], the authors explore the potential of reducing the number of active elements in antenna arrays while preserving desired properties through the use of sparse antenna arrays. In references [15] and [16], the authors investigate the feasibility of achieving the same goal with non-uniform antenna arrays. Studies [17] and [18] delve into the utilization of antenna arrays with parasitic elements. Particularly in the context of interplanetary missions conducted by small satellites, there is frequent discussion regarding the adoption of deployable reflective arrays [19]. These arrays, devoid of feeding line networks, solely reflect and collimate the signal from the primary emitter. Some sources, such as [20] and [21], investigate the feasibility of implementing beamforming on these reflective arrays solely by adjusting the impedance load of the individual elements on the reflective surface, without the necessity of phasing the transmitted or received signals.

The design of antenna arrays often involves the synthesis of their control. Many approaches address this challenge, as discussed in [22]. Deterministic methods, such as Chebyshev Array Synthesis, Synthesis by Fourier Transform, Sampling, and Root Matching, primarily focus on synthesizing the Array Factor. However, they don't consider the mutual coupling between elements and other sources of uncertainty. Additionally, these deterministic methods may not be suitable for non-uniform and sparse arrays.

Control synthesis can also be seen as an optimization task. This approach can incorporate full-wave models or even real devices. However, optimization methods are computationally demanding. Another category comprises Orthogonal Methods, which require significantly less computational power. They are well-suited for non-uniform arrays and can handle all features present in the full-field model. An emerging challenge is the development of methods capable of handling quantized control in both amplitude and phase. In recent times, there has been a significant focus on the digital control of antenna arrays [23]. Considerable attention has been directed towards phase control using a relatively small number of bits [24], [25].

The efficiency of the orthogonal method has been demonstrated for continuous control in several publications [22], [26], [27], [28]. Results are often depicted using radiation patterns obtained from proprietary code or full-wave simulations. However, in the case of antenna arrays with significant mutual coupling and integrated electronic components, simulation results should be complemented by experimental verification. In such scenarios, simulations may not yield accurate results due to the limited precision of the models used for substrates and electronic components. Simplified simulation methods are often employed to reduce computational complexity in large antenna arrays, but this can lead to inaccuracies when neglecting mutual couplings, which can significantly impact the simulation's accuracy. As a result, precise control of antenna array beamforming may necessitate the implementation of calibration and self-calibration. In references [29] and [30], the authors explore various approaches to calibrating antenna arrays.

To facilitate the development and experimental verification of antenna arrays, we have designed an advanced RF frontend unit capable of not only modifying the amplitude and phase of the signal for individual elements of the array but also disconnecting and loading these elements with variable impedance, enabling them to function as tuneable parasitic elements within the array. Simultaneously, it is possible to inject a direct current into the RF path to control the PIN diodes integrated directly into the individual elements of the array. Here, this is utilized to change the polarization at the level of the individual elements. The proposed antenna array testbed was measured in an anechoic chamber and compared with the simulated results.

This paper investigates the challenges and advancements in the design and control synthesis of antenna arrays with beamforming, addressing issues such as complexity, quantized control, and the need for experimental verification, and presents an advanced RF frontend unit for experimental validation in an anechoic chamber.

The work is organized as follows: Section II presents the methodology of research with prerequisites in antenna design, the synthesis of control, and the quantization effect. Section III explores the designs of the individual radiating elements of the array and the topology of the entire array. Proposed radio frequency frontends are discussed in Section IV. Section V describes the results of antenna array measurements in an anechoic chamber. The final section concludes the results of this work and outlines the direction of our next research in this area.

II. METHODOLOGY

The goal was to develop an experimental testbed of a reconfigurable antenna array. This testbed would allow us to address various critical issues, including the impact of quantized control on beamforming precision and null placement, the validity of synthesis methods in the presence of mutual coupling, and for further utilization of parasitic elements to simplify feeding of arrays. Therefore, this work comprises the following steps:

- Designing an antenna array with reconfiguration capability and advanced radio frequency frontends. This is described in detail in sections III and IV.
- Conducting a study on control synthesis based on orthogonal methods to simplify the implementation of real-time controlled beamforming.
- Investigating the effects of quantized control and parasitic elements utilization on simplification of arrays and radiation diagram properties.

This article contains only the sections related to the design and verification of the testbed for testing the mentioned issues, which are briefly summarized and will be further elaborated in upcoming various journal papers.

A. ANTENNA DESIGN

Considering our intended future application, which involves a ground station for small radio amateur satellites based on antenna arrays, it is essential that the antenna array be designed to operate within the 2400 MHz frequency band. Moreover, we require the capability to switch the polarization between left-hand and right-hand circular at the individual element level, achieved through a control signal injected into the RF signal path by the proposed frontends. In order to enhance the versatility of antenna array testing, we have introduced a digitally controlled load feature. This addition provides us with the capability to control the parasitic elements within the array, further increasing its versatility.

B. INFLUENCE OF QUANTIZATION

The influence of quantization on radiation patterns was studied mainly in connection with digital phase shifters. In [31], formula was derived formula for calculation of parasitic lobes caused by different methods of quantization. For round-off quantization it holds

$$\Delta\alpha = \frac{2\pi}{2^p}, \tag{1}$$

where $\Delta\alpha$ is the smallest possible step in steering angle and p is number of bits of the phase shifter. On the assumption that error is uniformly distributed in the interval

$$\left\langle \frac{-\pi}{2^p}, \frac{\pi}{2^p} \right\rangle,$$

the level of the largest parasitic sidelobe is

$$L \approx 20\log\left(\frac{\delta}{\pi-\delta}\right) = 20\log\left(\frac{\pi/2^p}{\pi-\pi/2^p}\right) = -6\cdot p\ [\text{dB}]. \tag{2}$$

There were proposed several methods of so-called randomizing of the phase error which further decrease the influence of quantization. For example, the level of parasitic side-lobes obtained using *Mean phase error equal to zero* is

$$L \approx -10\cdot p\ [\text{dB}]. \tag{3}$$

Note that the expressions above provide a good approximation for larger arrays. Even for smaller arrays, however, it is possible to state that the quantization error is significant for the low number of quantization levels $p \leq 3$, which is in accordance with results published in [32]. Fig. 1 shows the influence of quantization. On the horizontal axes is elevation angle, where required elevation is 20°. On the vertical axes is the array factor, where particular curves were obtained by quantization to the given number of bits (see the legend).

The quantization was performed using the formula

$$\hat{I}_\text{m} = \lfloor I_m \cdot 2^n \rfloor / 2^n, \tag{4}$$

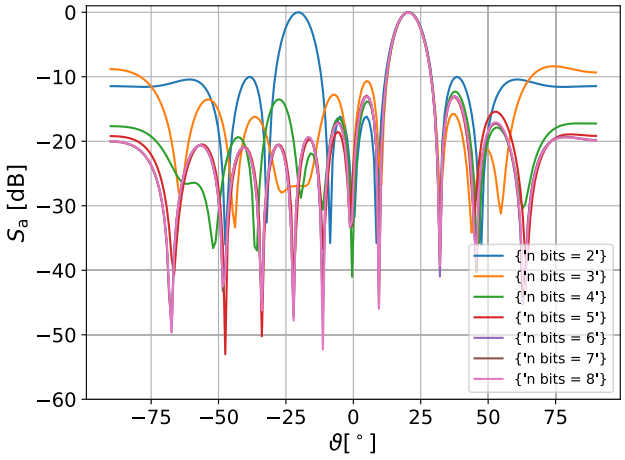

FIGURE 1. Influence of quantization on array factor for a beam steered to 25°. The array considered here is of 9 × 9 elements with spacing of 0.8λ.

where $\hat{I}_\text{m}$ is the quantized weight, I_{mn} is the normalized weight and symbols $\lfloor\rfloor$ are used for rounding.

$$\hat{\varphi} = \lfloor \varphi/\pi \cdot 2^n \rfloor / 2^n \cdot \pi. \tag{5}$$

The quantized magnitude and the quantized phase are directly used in simulations as weights for control excitation and in practical realization they are interpreted as n-bits words used for control of digital attenuators or phase sifters, respectively.

III. ARRAY DESIGN

The element of the array shown in Fig. 2a is based on the paper [33]. It is designed for a center frequency of 2450 MHz, consists of 3 × 3 elements, and can provide both LHC and RHC polarizations by switching ON or OFF DC voltage across appropriate PIN diodes. Two inductors in series (in total 36 nH) behave as an RF choke for this purpose. The patch motive of the element is printed on 0.762 mm thick substrate Rogers RO4350B ($\varepsilon_\text{r} = 3.66$, $\tan\delta = 0.0037$). Dimensions of the patch are: $R_1 = 7.15$ mm, $R_2 = 8.47$ mm, $R_3 = 22.60$ mm, $L = 11.93$ mm, $W = 3.49$ mm. The substrate is located $H = 11$ mm above the ground plane and supported by Teflon rods with $D_\text{S} = 6$ mm. Furthermore, the patch is fed through an impedance transformer shown in Fig. 2b of dimension $D_1 = 1.28$ mm, $D_2 = 3$ mm, $D_3 = 11$ mm, $H_1 = 3.6$ mm, $H_2 = 10$ mm.

Actual PIN diodes have been measured at a frequency of 2450 MHz and their equivalent circuit extracted. The ON state is represented by a series RL circuit with resistance $R = 0.334\ \Omega$ and inductance $L = 78.87$ nH. The values of RL circuit remain stable for various tested values of DC currents across the diodes. The OFF state is represented by a parallel RC circuit with $R = 4.163\ \text{k}\Omega$ and $C = 16.1$ pF. It has been further found that the antenna behavior is quite sensitive to this parallel capacitor.

For simplicity, only an array consisting of 3×3 elements as seen in Fig. 2c is considered. The size of the whole substrate is

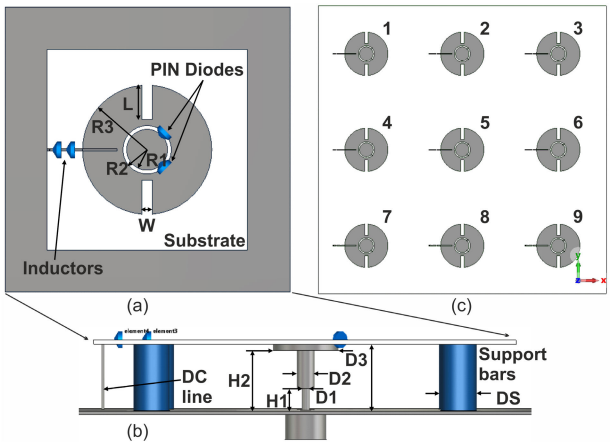

FIGURE 2. (a) Top and (b) side view of the dual-polarized array element. (c) Top side of 3 × 3 antenna array.

300×300 mm ($2.45\lambda_0$) and interelement spacing is 100 mm ($0.82\lambda_0$). The spacing is a little bit higher than usual in order to reduce mutual coupling between the elements.

IV. RF SIGNAL PATH

The primary function of the antenna array is beamforming, wherein RF frontends adjust signal amplitudes and phase shifts based on control synthesis, distributing them to the individual elements of the array. Phase shifters and attenuators are typically passive circuits with their inherent losses, leading to signal-to-noise ratio degradation. Therefore, our frontend for each antenna element includes active components, such as a low noise amplifier (LNA) and a power amplifier (PA), to mitigate signal degradation caused by insertion losses. Additionally, it incorporates receive/transmit (Rx/Tx) switches to enable the half-duplex operation of the proposed antenna array. However, modern beamforming frontends are required to offer a wider range of options beyond merely modifying the amplitude and phase of the signal. They must also support defined impedance loading, especially when it is necessary to deactivate specific antenna elements, such as in non-uniform antenna arrays or arrays with parasitic elements. Non-uniform arrays and arrays with parasitic elements have been used in some previously referenced publications to simplify array configurations. In certain applications, the ability to switch the polarization of individual elements within the array is also crucial. In our project, we endeavored to design a versatile antenna beamforming frontend capable of meeting a wide range of requirements necessary for experimental testing.

A. RF FRONTENDS - DESIGN AND CONTROLLING

The entire RF signal path system comprises a single electronic controlling board (block diagram in Fig. 3 top, circuit design of selected parts in Fig. 4 and 5) and nine controlled frontends (block diagram in Fig. 3 bottom) distributed across the three sub-boards connected to the back of the antenna array. The electronic control board

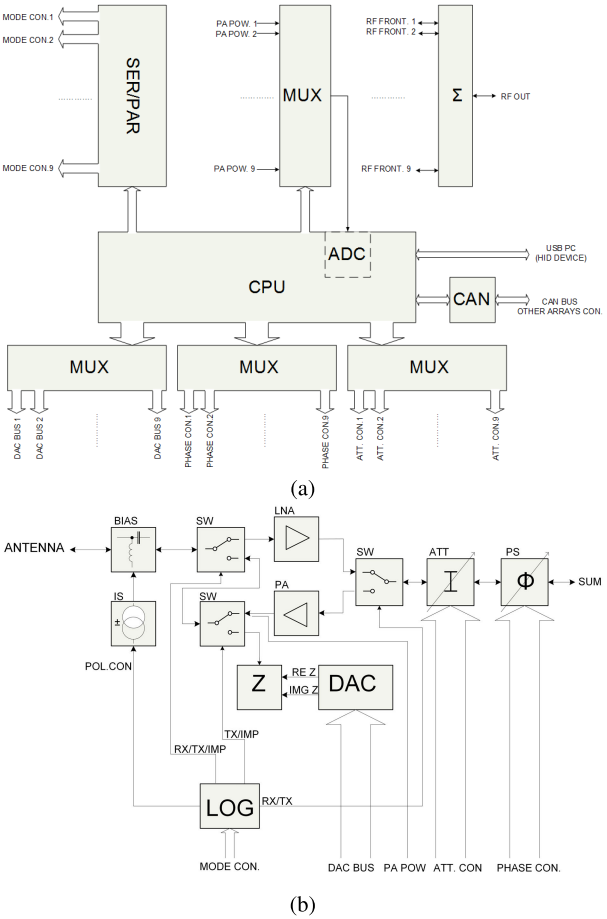

FIGURE 3. Block diagram of electronics for antenna array control and feeding: a) electronic control board and b) one of controlled RF frontend.

serves as an interface between a personal computer and the individual components of all frontends. Each frontend includes controlled Rx/Tx/impedance switches for mode selection, a PIN diode switch for polarization changes, a programmable load for impedance matching, digitally controlled phase shifters and attenuators for beamforming, a low noise amplifier in the Rx path for signal-to-noise ratio improvement, and a power amplifier in the Tx path to increase output power.

While the circuit design of the electronic control board may not significantly impact the radiation properties of the proposed antenna array, it plays a crucial role in the practical implementation of large antenna arrays. In such arrays, many individual components, including phase shifters, attenuators, switches, and programmable loads, must be controlled within a limited time frame to maintain the dynamic properties of beamforming, as required for specific applications. Moreover, there exists a constraint on the number of available input/output pins on the microcontrollers. To address these challenges, the solution leverages a relatively common microcontroller from the STM32 family, complemented by logic circuits from the 74HC154 series, which serve as multiplexers for control signals.

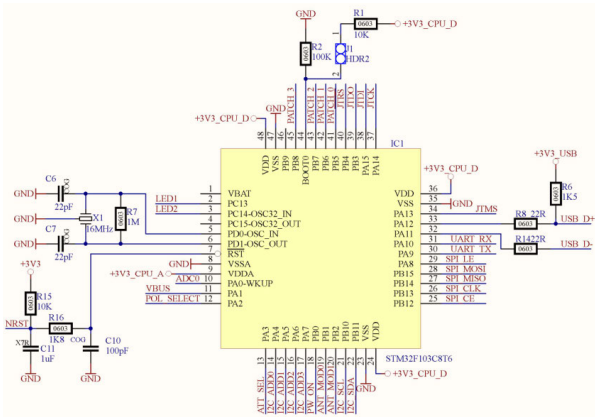

FIGURE 4. Circuit design of microcontroller part of the electronic control board.

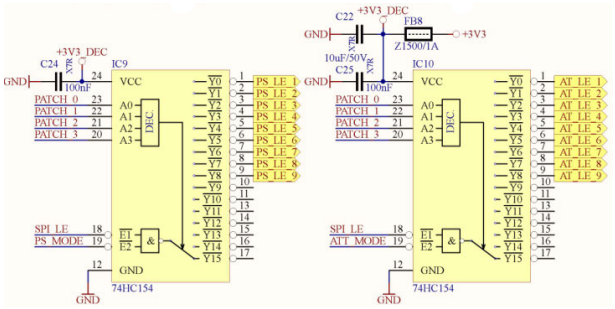

FIGURE 5. Circuit design of multiplexer part of the electronic control board.

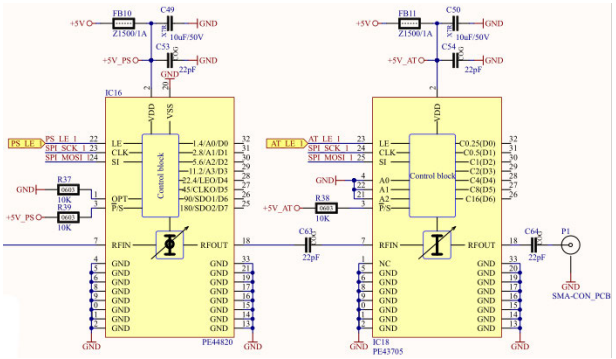

FIGURE 6. Circuit design of amplitude and phase signal conditioning.

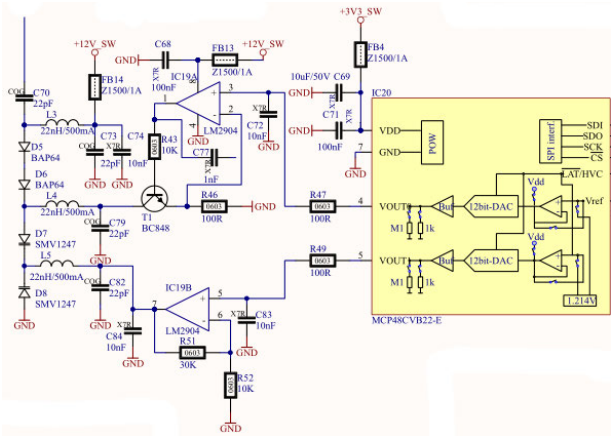

FIGURE 7. Circuit design of variable impedance load.

The signal path solution is founded on a custom design of frontends, employing key integrated circuits such as the Qorvo QPC9314. These QPC9314 chips serve a dual purpose, functioning both as Low Noise Amplifiers (LNA) and as switches between the Receiver (Rx) and Transmitter (Tx) or Impedance (Imp) functionalities in the design. In addition, we incorporate the Qorvo RFFM4200 for Power Amplification (PA) and switching between Tx and Imp modes, along with Peregrine Semiconductor's PE44820 digitally controlled phase shifters and PE43705 step attenuators for precise signal conditioning. Furthermore, our system accommodates the injection of control signals for polarization modification directly into the RF signal path, ensuring delivery to each antenna element. The block diagram of individual frontend is shown in Fig. 3 bottom, while circuit designs of selected parts are shown in Fig. 6 and 7.

The variable impedance loads are constructed by connecting PIN diodes, specifically the BAP64, in series for altering the real part of impedance. This adjustment is achieved through serial current regulation. In addition, serial varactors, specifically the SMV1247, are employed to modify the imaginary part of impedance, accomplished by tuning the cathode-anode voltage. To control these elements effectively, both current and voltage sources are powered by a dual 14-bit D/A converter integrated into the microcontroller section of the control board.

Polarization control is achieved through the utilization of two PIN diodes, which serve as switches and are directly integrated into all patch elements of the antenna array. A switching signal, in the form of a DC current, is generated within a circuit controlled by the microcontroller on the control board. This signal is then injected into the RF signal path through a bias-tee and delivered to patch elements. The details of the RF signal path design and circuit solution have been previously published in our prior paper [34] and, therefore, will not be expounded upon in this paper. Instead, we focus on discussing the measured properties in next chapter, as they hold significance in ensuring beamforming accuracy. To provide a visual representation, Fig. 8 illustrates the prototype of the electronic control board, along with the three sub-boards, each equipped with three assembled frontends (totally 9 frontends), all connected with the proposed antenna array from back side.

B. RF FRONTENDS - DISCUSSION OF PROPERTIES

An important aspect of antenna array control is having a deep understanding of the actual properties of antenna elements and their associated RF frontends. This knowledge is crucial because numerous adjustable parameters, especially amplitudes and phases, exhibit dependencies arising from

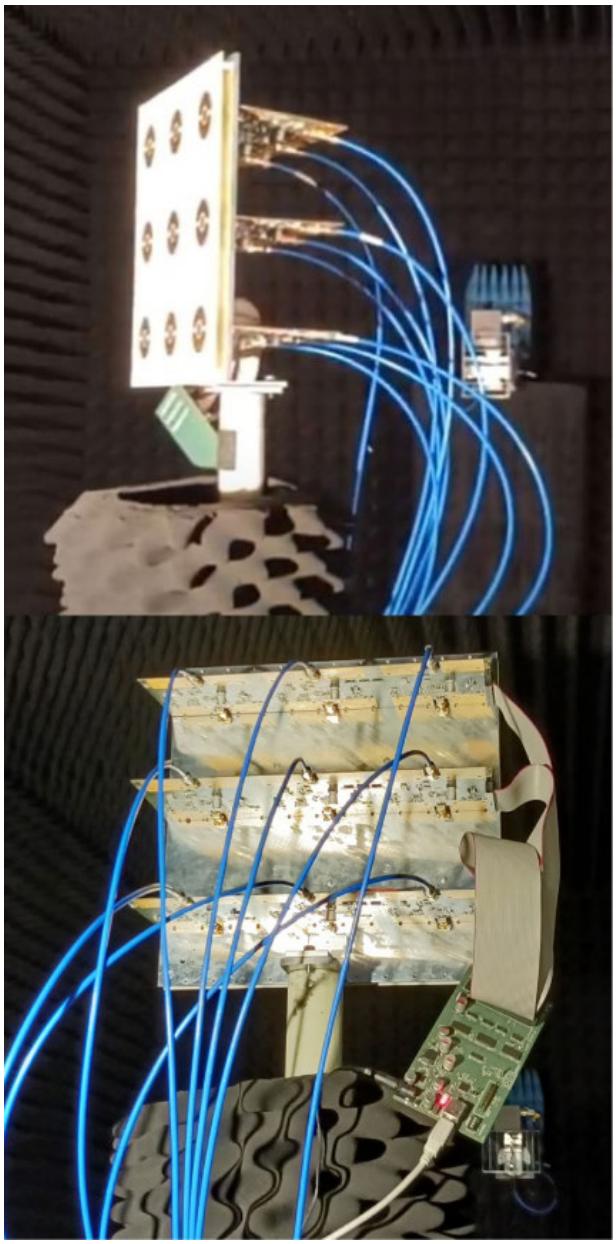

FIGURE 8. RF frontends with digital control board connected to the proposed antenna array during tests in anechoic chamber.

non-ideal properties of switches, mutual couplings, the variations of internal configurations of circuits during phasing and attenuating of signal, and variations of properties with the frequency. This is why many researchers are engaged in the development of effective calibration methods for large antenna arrays.

The range of measurements was carried out on the prototypes of the proposed RF frontends to analyze properties that affect the beamforming accuracy of the whole antenna array. We are focusing on four key issues:

- Dependence of properties of RF frontends on the frequency.
- Mutual dependencies between phase and amplitude if one of these parameters is modified.

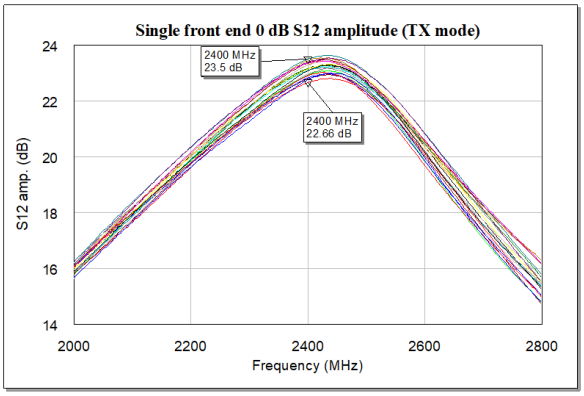

(a)

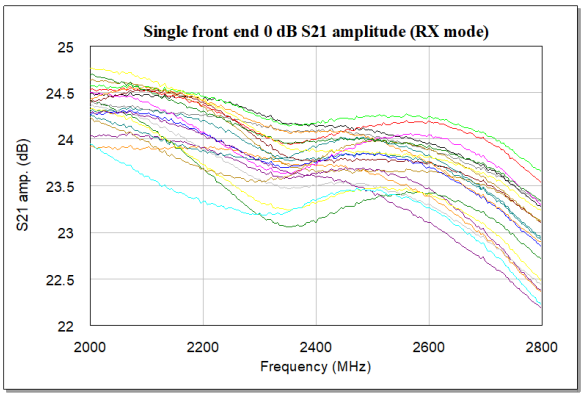

(b)

FIGURE 9. Measured variability of amplitudes on the frequency and on required phase shift (each color represents modification of phase shift with step 19°). (a) Transmitting mode, step attenuator set to 0 dB. (b) Receiving mode, step attenuator set to 0 dB.

- The accuracy of the step attenuators and phase shifters.
- Disparities between individual RF frontends.

Fig. 9a shows the dependence of amplitudes (whole gain of Tx signal path) on the frequency and also mutual dependence of amplitude and phase shift. Even if we consider a relatively narrow band of dedicated radio-amateur satellite communication from 2400 MHz to 2450 MHz, the variability of amplitude can reach up to 0.5 dB along this band. This figure also shows the mutual dependence between output amplitude and setable phase shift, which can reach approx. 1 dB for the whole supported range of phase shifts at operating frequency 2400 MHz.

Similar dependencies are visible also in receiving mode of RF frontends (Fig. 9b), however the whole gain of Rx signal path is more stable along the wider frequency band as the power amplifiers in Tx signal path have to be optimized to particular frequency.

Almost ideally linear dependency of phase shift on frequency is common property of digitally controlled phasing circuits and it is shown in Fig. 10a and 10b. However, the phase shift is also affected by modification of inner structure of step attenuator circuit during adapting amplitude of signal. These mutual dependencies between phase shift and setable

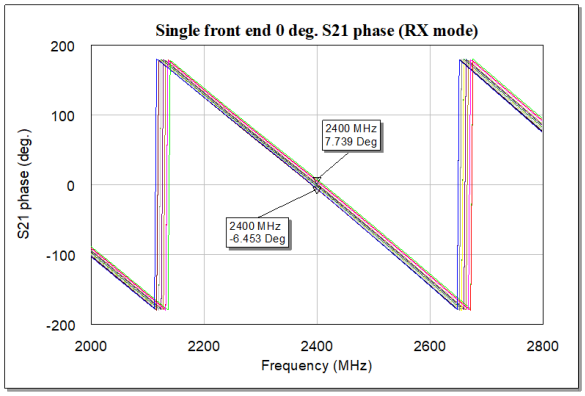

(a)

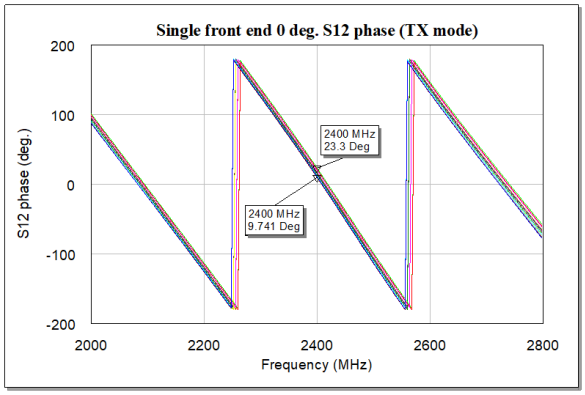

(b)

FIGURE 10. Measured variability of phase shift on the frequency and on required attenuation (each color represents modification of attenuation with step 2.5 dB). (a) Receiving mode, phase shift set to 0°. (b) Transmitting mode, phase shift set to 0°.

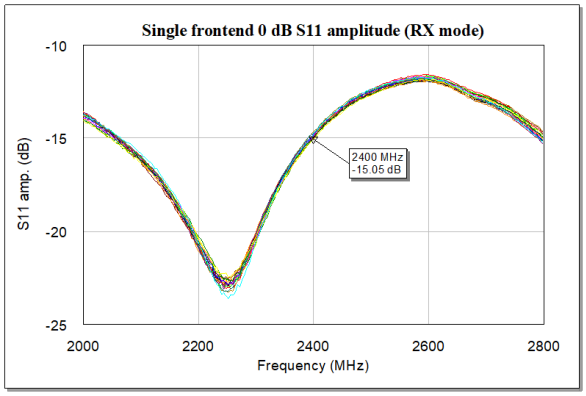

(a)

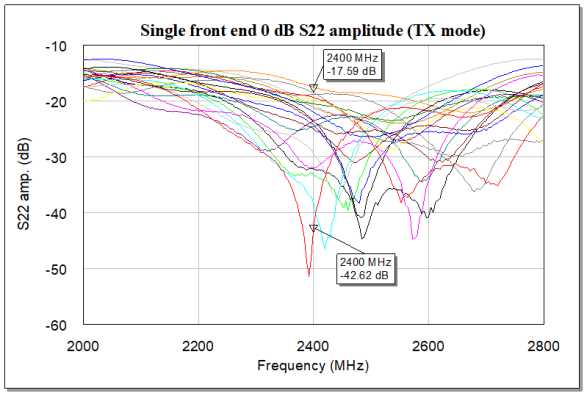

(b)

FIGURE 11. Measured variability of input return loss on the frequency and on required phase shift (each color represents modification of phase shift with step 19°). Receiving mode, step attenuator set to 0 dB. (b) Transmitting mode, step attenuator set to 0 dB.

attenuation are also well visible in Fig. 10a and 10b, where the phase shift can vary approx. 14° along the range of attenuation (30 dB in the developed digitally controlled step attenuator) in receiving and also in transmitting mode of RF frontends.

The input return loss s_{11} and the output return loss s_{22} of the RF frontends in receiving mode have completely different behaviour of dependencies on the frequency and setable phase shift based on the position of phasing circuit in the signal path. We can see a relatively small dependencies of input return loss (Fig. 11a) around working frequency 2400 MHz on both frequency and phase shift, because this impedance matching is given mainly by low noise amplifier in the signal path and not by inner structure of phasing circuit during modification of phase shift. On the other hand, the output return loss (Fig. 11b) have strong dependencies on both frequency and adjustable phase shift. This is because the phase shifter is directly placed at the output of RF frontend (in the meaning of Rx mode), not insulated by active amplifier. Consequently, modifications of the inner structure of the phasing circuit during phase shifting have direct impact on impedance matching.

The input return loss s_{11} and the output return loss s_{22} of the RF frontends in transmitting mode behave inversely to receiving mode. We observe relatively small dependencies in the output return loss (Fig. 12b) around working frequency 2400 MHz on both frequency and phase shift. This is primarily because impedance matching is given mainly by the power amplifier in the signal path, rather than the inner structure of the phasing circuit during adjustment of phase shift. The input return loss (Fig. 12a) exhibits strong dependencies on both frequency and adjustable phase shift. This is due to fact that the phase shifter is directly placed at the input of RF frontend (in the meaning of Tx mode), not insulated by active amplifier. As a result, modifications of the inner structure of the phasing circuit during phase shifting have a direct impact on impedance matching.

The behaviour of input and output return loss is influenced by the Tx/Rx signal path topology, particularly by the relative position of the phase shifter, step attenuator and active amplifier in the signal path (Fig. 3b). While results in Fig.9a up to Fig. 12b are plotted for individual RF frontends, it is also crucial to account for imbalances between all RF frontends for beamforming accuracy and compensate for them through calibration. To achieve this, a series of measurements was conducted to analyze the differences between individual RF frontends. Due to limited range of paper, only differences in the Tx mode are presented for clarity.

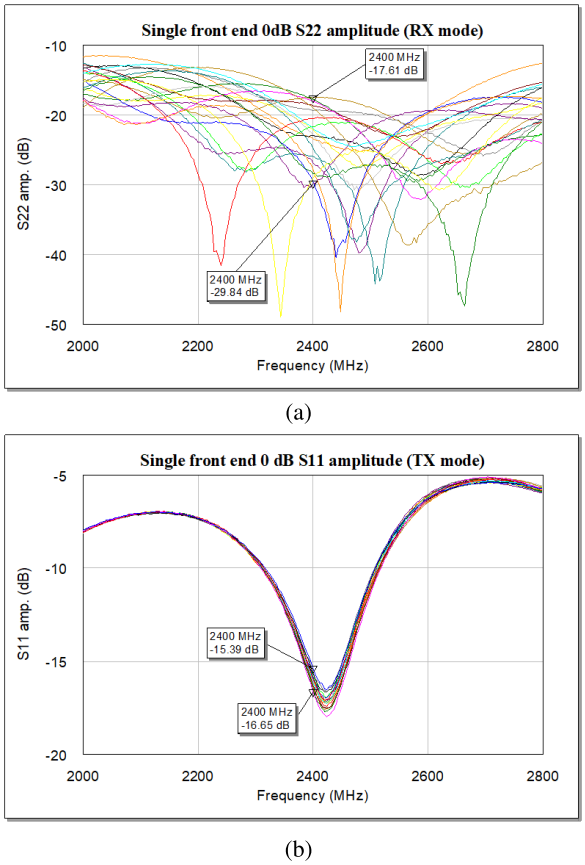

FIGURE 12. Measured variability of output return loss on the frequency and on required phase shift (each color represents modification of phase shift with step 19°). Receiving mode, step attenuator set to 0 dB. (b) Transmitting mode, step attenuator set to 0 dB.

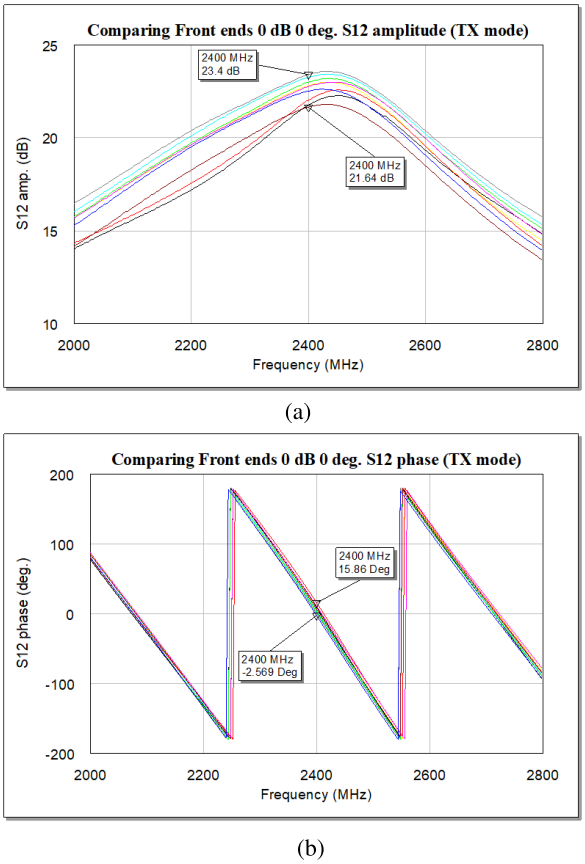

FIGURE 13. Measured differences of output amplitude (a) and phase (b) between individual RF frontends (individual RF frontends are separated by color) - transmitting mode, step attenuator set to 0 dB and phase shifter is set to 0°.

In Fig. 13a, we observe the differences in output amplitudes among the nine implemented RF frontends operating in Tx mode, with 0 dB attenuation set in the attenuator circuit and a 0° phase shift in the phasing circuit. At the operating frequency of 2400 MHz, the amplitudes differ by approximately 1.8 dB, and the frequency-dependent variations in amplitudes are visible for each individual frontend. In Fig. 13b, we can see the differences in output phase shifts among the nine RF frontends operating in Tx mode, with 0 dB attenuation set in the attenuator circuit and a 0° phase shift in the phasing circuit. At the operating frequency of 2400 MHz, the phase shifts differ by approximately 18.4°. Differences in the output and input return loss of RF frontends are shown in Fig. 14a and 14b. Both characteristics demonstrate strong variability among the nine realized RF frontends, especially within the optimized frequency band around the operating frequency of 2400 MHz. However, the values of return loss are sufficient even for the worst-case scenario and do not affect the performance of the entire array antenna.

In addition to the properties mentioned above, the overall performance of RF frontends in real applications is also dependent on the achieved output power and input noise figure. Active amplifiers, such as LNA and PA, help to overcome power limitations of phasing and attenuating circuits and their losses. While the precise characteristics of the proposed frontends are beyond the scope of this work, it is noteworthy that we achieved 20 dBm of output power in Tx mode per one RF frontend. In Rx mode, the noise figure of the RF frontends was approximately 1.3 dB around the operating frequency of 2400 MHz.

V. MEASUREMENTS OF ANTENNA ARRAY

To verify the accuracy of the design and simulation methods, to study the influence of quantized control and effective calibration methods, a prototype of a 3 × 3 antenna array was manufactured and assembled by RF frontends, including the digital control part. Verification of the entire antenna array took place in the specialized facility of the shielded anechoic chamber, firstly over the individual elements of the array, and later over the entire antenna array excited by the controlled RF frontends to verify the possibilities and accuracy of beamforming during quantized control. As a receiving antenna, a DRH10 horn by RFSpin [35] has been used. The antenna has been axially rotated in order to obtain

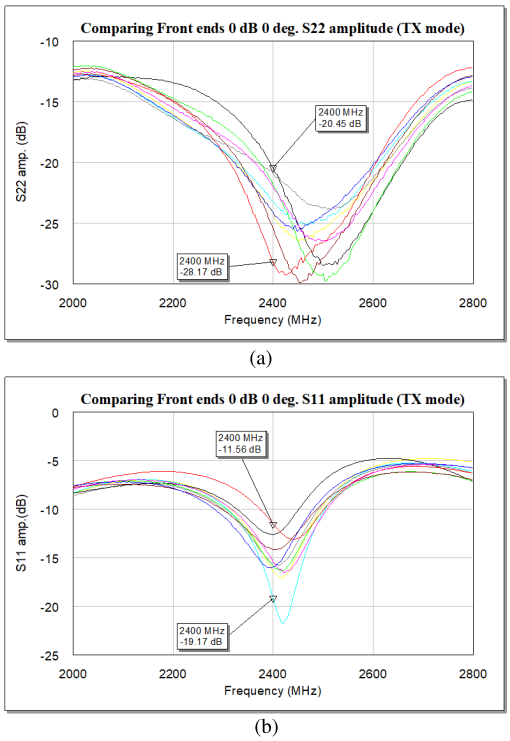

FIGURE 14. Measured differences of input (a) and output (b) return loss between individual RF frontends (individual RF frontends are separated by color) - transmitting mode, step attenuator set to 0 dB and phase shifter is set to 0°.

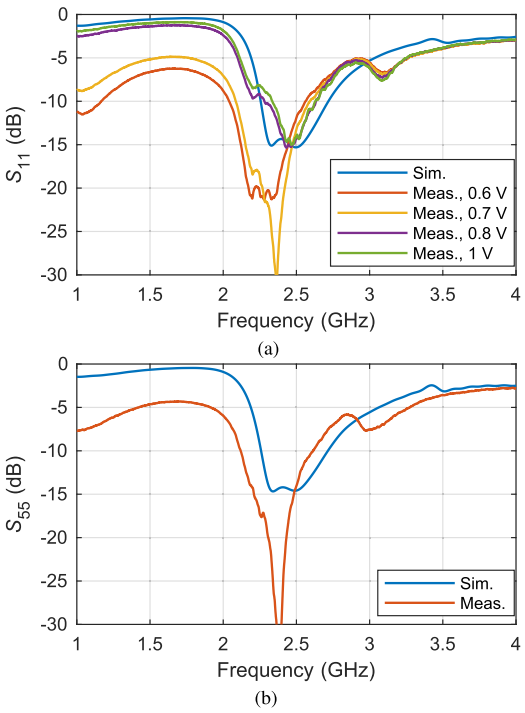

FIGURE 15. Simulated and measured reflection coefficients for left-handed polarization of antenna array elements: (a) 1 and (b) 5. Numbering of the elements is according to Fig. 2.

all the polarization components from which the LHC/RHC patterns were evaluated.

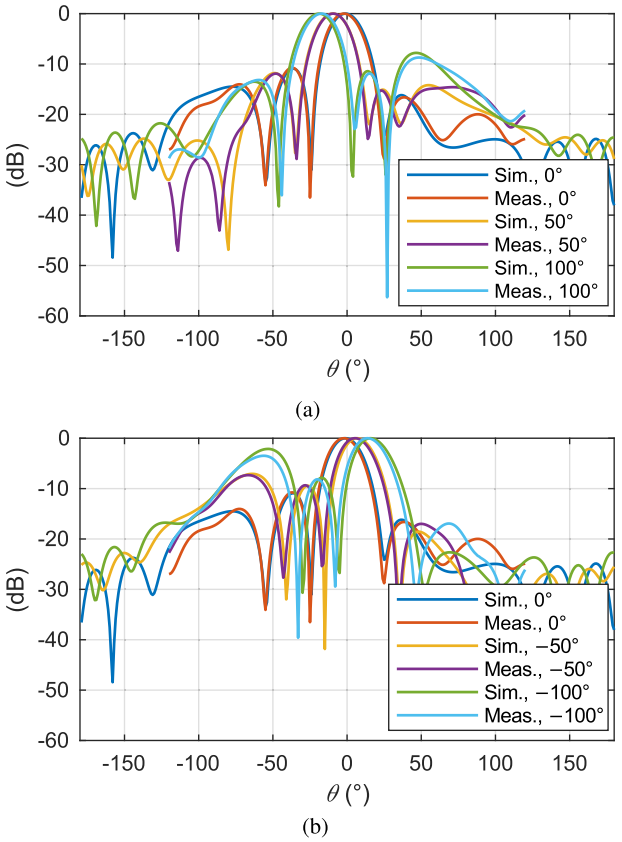

FIGURE 16. Simulated and measured radiation patterns for left-handed polarization of antenna array elements and amplitude and phase excitation $|\mathbf{v}| = [1, 1, 1, 1, 1, 1, 1, 1, 1, 1]$ and $\angle(\mathbf{v})$: 0° : [0°, 0°, 0°, 0°, 0°, 0°, 0°, 0°, 0°, 0°], 50° : [0°, 0°, 0°, +50°, +50°, +50°, +100°, +100°, +100°], 100° : [0°, 0°, 0°, +100°, +100°, +100°, +200°, +200°, +200°], −50° : [0°, 0°, 0°, −50°, −50°, −50°, −100°, −100°, −100°], −100° : [0°, 0°, 0°, −100°, −100°, −100°, −200°, −200°, − 200°].

A. MEASUREMENTS OF INDIVIDUAL ELEMENTS IN ARRAY

First, one element was excited from RF generator and the rest loaded by 50 Ohm impedance during measurements. Frequency dependence of the reflection coefficients S_{mm} and antenna gain was measured in each of antenna elements for both polarization (RHC, LHC) and compared to simulation. Since they are very similar, we show for clarity only the LHC results, see Fig.15. The differences are most likely attributed to the PIN diode model limitations, particularly for its variations with the DC voltage. This is clearly illustrated in Fig.15a.

B. MEASUREMENTS OF ARRAY EXCITED BY RF FRONTENDS

Finally, the complete antenna array, along with the connected RF frontends, underwent measurement within an anechoic chamber to validate its beamforming capabilities under quantized control and to assess its polarization switching functionality. Again, for clarity, we show only the LHC results as the RHC is very similar, see Fig.16. We've used constant amplitudes and progressive phasing along the elements to obtain the radiation pattern steering.

The excitation vector has constant amplitudes $|\mathbf{v}| = [1, 1, 1, 1, 1, 1, 1, 1, 1, 1]$ and the phase is progressive starting with $\angle(\mathbf{v}) = [0°, 0°, 0°, 0°, 0°, 0°, 0°, 0°, 0°, 0°]$ (broad-side radiation) and then using 50° step, see Fig. 16.

VI. CONCLUSION

The presented study successfully undertook the design, realization, and verification of an antenna array, producing several interesting outcomes. At first, the study represents a proof of concept of the design of an antenna array. The antenna array is fully functional and operational. The full-wave simulation results are in good agreement with the experiments. This allows the successful application of the orthogonal method to control synthesis. The necessity of a two-stage calibration of the entire device was shown. The first step on the level of the frontends is successfully fulfilled. The second step, calibration on the whole antenna array, is the subject of further research.

It also has to be noted that all measured results of RF frontend properties indicate that the mutual dependencies between the set output amplitude and set output phase shift are not negligible. These dependencies could potentially impact the accuracy of beamforming and the side lobe attenuation of the antenna array radiation diagram. Additionally, variations among individual RF frontends could have a similar effect. Therefore, in situations where precise beamforming and side lobe attenuation are required, it become essential to analyze and calibrate these properties, taking into account also their frequency dependence. However, in such cases, the complexity of calibration can be substantial due to the numerous discrete values of attenuation, phase shift, frequency steps, and the high number of RF frontends present in large arrays, all of which need to be measured and calibrated.

Future work in this area could explore further advancements in antenna array design and control synthesis, potentially focusing on enhancing the efficiency and scalability of large-scale arrays, developing novel methods to address quantized control challenges, and investigating innovative calibration techniques for improved accuracy in simulations and experimental verifications. Additionally, research could explore the integration of emerging technologies, such as machine learning or artificial intelligence, to optimize the performance of antenna arrays in diverse applications and environments.

REFERENCES

[1] S. Xia, Q. Jiang, C. Zou, and G. Li, "Beam coverage comparison of LEO satellite systems based on user diversification," *IEEE Access*, vol. 7, pp. 181656–181667, 2019.

[2] M. Schneider, C. Hartwanger, and H. Wolf, "Antennas for multiple spot beam satellites," *CEAS Space J.*, vol. 2, nos. 1–4, pp. 59–66, Dec. 2011.

[3] D. Srinivasan, R. Vaughan, R. Wallis, M. Mirantes, T. Hill, S. Cheng, J. Bruzzi, and K. Fielhauer, "Implementation of an X-band phased-array subsystem in a deep space mission," in *Proc. IEEE Aerosp. Conf.*, Mar. 2005, pp. 1541–1551.

[4] V. Vilnrotter, M. Quadrelli, R. Hodges, S. Bandyopadhyay, S. Finley, and D. Kahan, "Experimental validation of swarm array results using Mars cube one (marco) a/b downlink signals," in *Proc. IEEE Aerosp. Conf.*, Mar. 2020 pp. 1–7.

[5] T. Joo, K. Kim, and J. Seo, "Design of tile-type Rx phased-array antenna for Ku-band satellite communications," *J. Korean Inst. Electromagn. Eng. Sci.*, vol. 30, no. 9, pp. 702–711, Sep. 2019.

[6] H. Schippers, J. Verpoorte, P. Jorna, A. Hulzinga, A. Meijerink, C. G. H. Roeloffzen, R. G. Heideman, A. Leinse, and M. Wintels, "Conformal phased array with beam forming for airborne satellite communication," in *Proc. Int. ITG Workshop Smart Antennas*, pp. 343–350, 2008. [Online]. Available: https://api.semanticscholar.org/CorpusID:5800995

[7] G. He, X. Gao, L. Sun, and R. Zhang, "A review of multibeam phased array antennas as LEO satellite constellation ground station," *IEEE Access*, vol. 9, pp. 147142–147154, 2021.

[8] N. Kaya, "Three dimensional phased array antenna for communications with satellite constellations," in *Proc. 15th Eur. Conf. Antennas Propag. (EuCAP)*, Mar. 2021, pp. 1–4.

[9] A. K. Vallappil, M. K. A. Rahim, B. A. Khawaja, N. A. Murad, and M. G. Mustapha, "Butler matrix based beamforming networks for phased array antenna systems: A comprehensive review and future directions for 5G applications," *IEEE Access*, vol. 9, pp. 3970–3987, 2021.

[10] M. Comisso, G. Palese, F. Babich, F. Vatta, and G. Buttazzoni, "3D multi-beam and null synthesis by phase-only control for 5G antenna arrays," *Electronics*, vol. 8, no. 6, p. 656, Jun. 2019. [Online]. Available: https://www.mdpi.com/2079-9292/8/6/656

[11] V. A. Kashin and I. S. Shurygina, "Synthesis of multibeam directivity patterns to improve performance of radar stations with an active phased antenna array," *J. Commun. Technol. Electron.*, vol. 66, no. 10, pp. 1155–1162, Oct. 2021.

[12] C. Sahin, P. M. McCormick, J. G. Metcalf, and S. D. Blunt, "Power-efficient multi-beam phase-attached radar/communications," in *Proc. IEEE Radar Conf. (RadarConf)*, Apr. 2019, pp. 1–6.

[13] W. Shi, Y. Li, L. Zhao, and X. Liu, "Controllable sparse antenna array for adaptive beamforming," *IEEE Access*, vol. 7, pp. 6412–6423, 2019.

[14] F. Yang, S. Yang, Y. Chen, S. Qu, and J. Hu, "Synthesis of sparse antenna arrays subject to constraint on directivity via iterative convex optimization," *IEEE Antennas Wireless Propag. Lett.*, vol. 20, no. 8, pp. 1498–1502, Aug. 2021.

[15] A. Soares and J. A. Santos, "Design and analysis of a non-uniform antenna array for IoT applications," *J. Commun. Inf. Syst.*, vol. 38, no. 1, pp. 144–148, 2023.

[16] A. Arce, E. Stevens-Navarro, M. Cardenas-Juarez, U. Pineda-Rico, and D. H. Covarrubias, "A coherent multiple beamforming network for a non-uniform circular antenna array," *Radioengineering*, vol. 27, no. 1, pp. 74–83, Apr. 2019.

[17] H. H. Tran and H. C. Park, "Gain and bandwidth enhancements of sequential-fed circularly polarized patch antenna array using multiple parasitic elements," *Int. J. RF Microwave Comput.-Aided Eng.*, vol. 30, no. 9, Sep. 2020, Art. no. e22319.

[18] D.-G. Seo and W.-S. Lee, "A multiply parasitic-coupled, three-dimensional antenna array with wide elevation angle for seamless uav communications," *The Appl. Comput. Electromagn. Soc. J. (ACES)*, pp. 461–465, 2020.

[19] R. E. Hodges, N. Chahat, D. J. Hoppe, and J. D. Vacchione, "A deployable high-gain antenna bound for Mars: Developing a new folded-panel reflectarray for the first CubeSat mission to Mars," *IEEE Antennas Propag. Mag.*, vol. 59, no. 2, pp. 39–49, Apr. 2017.

[20] H. Yang, F. Yang, S. Xu, Y. Mao, M. Li, X. Cao, and J. Gao, "A 1-Bit 10 × 10 reconfigurable reflectarray antenna: Design, optimization, and experiment," *IEEE Trans. Antennas Propag.*, vol. 64, no. 6, pp. 2246–2254, Jun. 2016.

[21] P. Nayeri, F. Yang, and A. Z. Elsherbeni, "Beam-scanning reflectarray antennas: A technical overview and state of the art," *IEEE Antennas Propag. Mag.*, vol. 57, no. 4, pp. 32–47, Aug. 2015.

[22] J. Sahalos, *Orthogonal Methods for Array Synthesis: Theory and the ORAMA Computer Tool*. Hoboken, NJ, USA: Wiley, Apr. 2006.

[23] S. Li, Y. Wang, and F. Xu, "1-bit coding reconfigurable array for 2-D wide-angle scanning," *IEEE Trans. Antennas Propag.*, vol. 71, no. 3, pp. 2421–2432, Mar. 2023.

[24] S.-Y. Li, Y. Wang, and F. Xu, "Two-bit planar coding reconfigurable array antenna for dual-polarized wide-angle beam scanning," *IEEE Trans. Antennas Propag.*, vol. 71, no. 9, p. 1, Sep. 2023.

[25] C. Deng, D. Liu, B. Yektakhah, and K. Sarabandi, "Series-fed beam-steerable millimeter-wave antenna design with wide spatial coverage for 5G mobile terminals," *IEEE Trans. Antennas Propag.*, vol. 68, no. 5, pp. 3366–3376, May 2020.
[26] M. G. H. Alijani and M. H. Neshati, "A new noniterative method for pattern synthesis of unequally spaced linear arrays," *Int. J. RF Microw. Comput.-Aided Eng.*, vol. 29, no. 11, Nov. 2019, Art. no. e21921.
[27] K. Marák, J. Kracek, and S. Bilicz, "Antenna array pattern synthesis using an iterative method," *IEEE Trans. Magn.*, vol. 56, no. 2, pp. 1–4, Feb. 2020.
[28] H. P. Kracek Jan and L. Tomas, "Beamforming for antenna array using modal technique," in *Proc. 16th Eur. Conf. Antennas Propag. (EuCAP)*, vol. 56, no. 2, 2022, pp. 1–4.
[29] E. Sippel, M. Lipka, J. Geiß, M. Hehn, and M. Vossiek, "In-situ calibration of antenna arrays within wireless locating systems," *IEEE Trans. Antennas Propag.*, vol. 68, no. 4, pp. 2832–2841, Apr. 2020.
[30] A. Nafe, K. Kibaroglu, M. Sayginer, and G. M. Rebeiz, "An in-situ self-test and self-calibration technique utilizing antenna mutual coupling for 5G multi-beam TRX phased arrays," in *IEEE MTT-S Int. Microw. Symp. Dig.*, Jun. 2019, pp. 1229–1232.
[31] M. Smith and Y. Guo, "A comparison of methods for randomizing phase quantization errors in phased arrays," *IEEE Trans. Antennas Propag.*, vol. AP-31, no. 6, pp. 821–828, Nov. 1983.
[32] D. Pánek, T. Orosz, P. Karban, D. C. D. Gnawa, and H. K. Neghab, "Performance comparison of quantized control synthesis methods of antenna arrays," *Electronics*, vol. 11, no. 7, p. 994, Mar. 2022.
[33] K. M. Mak, H. W. Lai, K. M. Luk, and K. L. Ho, "Polarization reconfigurable circular patch antenna with a C-shaped," *IEEE Trans. Antennas Propag.*, vol. 65, no. 3, pp. 1388–1392, Mar. 2017.
[34] M. Pokorny, I. Vertat, and J. Masopust, "Electronic control board for phased antenna array research and prototyping," in *Proc. Int. Conf. Appl. Electron. (AE)*, Sep. 2022, pp. 1–6.
[35] Rfspin. Accessed: Jan. 15, 2024. [Online]. Available: http://www.rfspin.com

MICHAL POKORNY received the Ing. and Ph.D. degrees in electronic engineering from the University of West Bohemia, Pilsen, Czech Republic, in 2003 and 2012, respectively. His research interests include radiofrequency and microwave circuits design and prototypes realization and measuring.

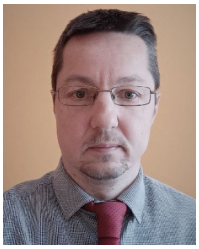

IVO VERTAT was born in Czech Republic, in 1980. He received the Ph.D. degree from the Faculty of Electrical Engineering, University of West Bohemia, in 2012. His doctoral thesis focused on developing efficient communication systems for picosatellites. He is an expert in wireless communication and space hardware design. Since 2009, he has been a member of the PilsenCUBE Team and worked on the university ground station. Since 2017, he has been operating the VZLUSAT-1, and since 2022, also the VZLUSAT-2 satellite. Additionally, he has involved in the feasibility study of the REMEC project–a mission of a small satellite planned for the Lagrange L2 point of the Earth–Sun system, using an advanced deployable reflectarray antenna to maintain a positive radio link budget for the limited aperture of the ground station dish antenna.

DAVID PANEK (Member, IEEE) received the master's and Ph.D. degrees in electronics from the University of West Bohemia, in 2001 and 2009, respectively. He is currently a Senior Researcher with the Research and Innovation Centre for Electrical Engineering and an Associate Professor with the Faculty of Electrical Engineering, Pilsen, Czech Republic, and also with the Department of Electrical and Computational Engineering, University of West Bohemia, Pilsen. His research interests include machine learning, numerical modeling, simulation and optimization, and antenna array design.

PAVEL HAZDRA (Member, IEEE) was born in Prague, Czech Republic, in 1977. He received the M.Sc. and Ph.D. degrees in electrical engineering from Czech Technical University in Prague (CTU), in 2003 and 2009, respectively. Since 2012, he has been an Associate Professor with the Department of Electromagnetic Field, CTU in Prague. He has authored or coauthored more than 120 journal and conference papers. His research interests include EM/antenna theory, electrically small antennas, reflector antennas and their feeds, and antennas for amateur radio purposes.

MILAN SVANDA received the M.S. and Ph.D. degrees in radioelectronics from Czech Technical University in Prague (CTU), Czech Republic, in 2007 and 2011, respectively. He is currently a Research Scientist with CTU. He is the author or coauthor of more than 60 papers published in international journals or conference proceedings and the coauthor of seven patents. His main research activities are focused on antennas operating in the close vicinity of the human body, low-profile and wearable RFID, chipless RFID systems, and sensor antennas.

JAN KRACEK (Member, IEEE) received the Ing. degree in telecommunications and radio engineering and the Ph.D. degree in radioelectronics from the Faculty of Electrical Engineering (FEE), Czech Technical University in Prague (CTU), Czechia. He is currently a Researcher with the Department of Electromagnetic Field, FEE. His research and teaching interests include electromagnetic field theory, antenna theory and design, wireless power transfer, RFID, electromagnetic sensors, higher symmetries, and artificial materials.

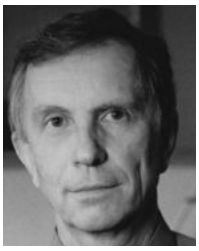

MILOS MAZANEK (Life Senior Member, IEEE) was born in Tanvald, Czech Republic, in 1950. He received the M.Sc. and Ph.D. degrees in electrical engineering from Czech Technical University in Prague (CTU), in 1975 and 1981, respectively. Since 1975, he has been with the Department of Electromagnetic Field, CTU in Prague, and the Department of Physics, Czech Academy of Science. He has authored or coauthored more than 90 journal and conference papers. His research interests include antennas, propagation, electromagnetic compatibility, remote sensing, and microwave radiometry.

JIRI MASOPUST was born in Czech Republic, in 1960. He received the Ing. degree in computer science from the University of West Bohemia, in 1984, and the C.Sc. degree in radio electronics from the Czechoslovak Academy of Science, in 1988. Since 1995, he has been an Associate Professor (doc.) of electronics from the University of West Bohemia, Pilsen. His publication, research activities, and projects are focused on the area of electronic communications (mobile phone systems and private mobile radio systems for rescue networks), satellite systems (project PilsenCUBE and VZLUSAT), medical electronics (patents in USA), and multimedia technology (cooperation with Panasonic).

PAVEL KARBAN (Member, IEEE) was born in 1979. He graduated from the Faculty of Electrical Engineering, University of West Bohemia, Pilsen, in 2002. He is currently a Professor with the University of West Bohemia. He is the author or coauthor of one monograph, one book on Matlab, about 60 articles in impact factor journals, and several large program packages. His H-index is 14. His research interests include computational electromagnetics, coupled problems, finite element method, and machine learning using AI.